Reconstruction of localized force distributions in cells and tissues from substrate displacements using physically-consistent regularization

Joshua C. Chang and Yanli Liu and Tom Chou
Epidemiology and Biostatistics Section, Rehabilitation Medicine, Clinical Center, The National Institutes of Health, Bethesda MD, 20892 and Depts. of Biomathematics and Mathematics, UCLA, Los Angeles, CA 90095-1766

We develop a method to reconstruct, from measured displacements of the underlying elastic substrate, the spatially dependent forces that cells or tissues impart on them. Since these sources of force typically arise from focal adhesions, with are localized or "compact," and discontinuous, we solve this inverse problem using methods of optimization useful for image segmentation. In addition to the standard quadratic data mismatch terms (that defines least-squares fitting), we motivate a term in in the objective function which penalizes variations in the tensor invariants of the reconstructed stress while preserving boundaries. By minimizing the objective function subject to physical constraints, we are able to efficiently reconstruct stress fields with localized structure from simulated and experimental substrate displacements. We provide a numerical method for setting up a discretized inverse problem that that is solvable by standard convex optimization techniques. Our method incorporates the exact solution of the forward problem accurate to first-order finite-difference approximation in the stress tensor. For utility with newly-available high-resolution data, we motivate the use of distance-based cutoffs for data inclusion and find under loose regularity conditions the reconstruction error that results.

./figures/Fig1.pdf

FIG. 1. A schematic of an isolated cell. (a) The boundary of the cell footprint is denoted by the dashed curve, the stress field is represented by the red regions that impart a stress $\mathbf{F}(x, y)$ on the surface. Displacements $\mathbf{u}(\mathbf{r}_i)$ of the elastic medium are measured at position $\mathbf{r}_i = x_i\hat{x} + y_i\hat{y} + z_i\hat{z}$ (blue dots) that can be inside or outside the cell footprint, on the surface ($z_i = 0$), or below the surface ($z_i < 0$). (b). A perspective view of the elastic substrate and cellular footprint.

INTRODUCTION

Cell motility and response to signals have hitherto almost always been studied in two-dimensional geometries in which cells are placed on a flat elastic substrate. Dynamic adhesion between the cells and the substrate are realized through *e.g.*, lamellapodia, filapodia, and dynamically reorganizing focal adhesions. Such structures are spatially localized, as shown in Fig. 1. Similarly, on larger length scales, a collection of cells can give rise to localized stress distributions. For example, the leading edge of a cell layer produces the pulling force that leads to migration in wound healing assays.

Dynamically varying force generating structures are often small and difficult to image, especially without biochemical modification such as incorporation of fluorescent dyes. Therefore, other methods for inferring their positions and magnitudes have been developed. The simplest method relies on measuring the displacement of fiduciary markers, such as gold nanoparticles, embedded in the elastic substrate [1]. The measured displacements are an indirect probe of the force-generating structures. Any inversion method should be able to not only reconstruct the positions and magnitudes of the stress field, but should ideally be able to capture potentially sharp boundaries of the stress-generating structures.

Therefore, we develop a novel method for elastic stress source recovery using ideas developed for image segmentation. This class of methods relies on optimization that uses an L^1 regularization term in the objective function. This type of regularization term is not derived from a fundamental physical law, but represents a prior knowledge that the function to be recovered is sparse in content except near edges. Nonetheless, our new objective will be constructed to obey physical constraints and symmetries.

In the next section, we review the basic linear equations of elasticity that describe the displacement field as a function of an arbitrary surface stress distribution. This model is then used to construct the data mismatch term in an objective function. We then motivate regularization and constraint terms to construct the full objective function. Finally, we demonstrate explore our method using experimental data. Our method provides good reconstruction of localized structures that exhibit desirable qualities such as the suppression of Gibbs ringing phenomenon at the boundaries of the stress structures.

ELASTIC MODEL

In this section, we explicitly describe the elastic green's function associated with a point force applied to the surface of a semi-infinite half-space, as shown in Fig. 1(b). The domain of the elastic medium is $\mathcal{D} = \{(x, y, z)|x, y \in R, z \leq 0\}$. We assume that the elastic medium is infinite in depth ($d \to \infty$) and lateral extent.

The Green's function

$$\mathbf{G^0} = \begin{bmatrix} G^0_{xx}(x,y,z) & G^0_{xy}(x,y,z) & G^0_{xz}(x,y,z) \\ G^0_{yx}(x,y,z) & G^0_{xy}(x,y,z) & G^0_{yz}(x,y,z) \\ G^0_{zx}(x,y,z) & G^0_{zy}(x,y,z) & G^0_{zz}(x,y,z) \end{bmatrix} \tag{1}$$

for linear isotropic elasticity theory in the half-space is given by its components

$$G^0_{ss}(x,y,z) = \frac{1+\nu}{2\pi E}\left[\frac{2(1-\nu)R_\perp - z}{R_\perp(R_\perp - z)} + \frac{[2R_\perp(\nu R_\perp - z) + z^2]s^2}{R^3_\perp(R_\perp - z)^2}\right], \tag{2}$$

$$G^0_{zz}(x,y,z) = \frac{1+\nu}{2\pi E}\left(\frac{2(1-\nu)}{R_\perp} + \frac{z^2}{R^3_\perp}\right), \tag{3}$$

$$G^0_{xy}(x,y,z) = G_{yx} = \frac{1+\nu}{2\pi E}\frac{[2R_\perp(\nu R_\perp - z) + z^2]xy}{R^3_\perp(R_\perp - z)^2}, \tag{4}$$

$$G^0_{sz,zs}(x,y,z) = \frac{1+\nu}{2\pi E}\left(\frac{sz}{R^3_\perp} \pm \frac{(1-2\nu)s}{R_\perp(R_\perp - z)}\right), \tag{5}$$

where $s = x, y$ the equation with $\pm$ corresponds to G^0_{sz} and G^0_{zs}, respectively, and $R_\perp \equiv \sqrt{x^2+y^2}$. The Young's modulus and Poisson ratio of the elastic substrate are denoted by E and ν, respectively. The displacement of a material point at $(x, y, z \leq 0)$ in the medium due to a stress distribution $\mathbf{F}$ is simply the convolution $\mathbf{u}(\mathbf{r}) \equiv [u_x\ u_y\ u_z]^\intercal = \mathbf{G^0} * \mathbf{F}$.

For our specific problem, we shall specialize the forces to surface stresses $\sigma_{x,y}$ that act on the plane perpendicular to the $\hat{z}$ axis. We define the in-plane stress distribution, at depth z, as $\boldsymbol{\sigma}(x, y, z) = \sigma_{xz}(x, y, z)\hat{x} + \sigma_{yz}(x, y, z)\hat{y}$. The resulting surface-level displacement fields become

$$u_x(x,y) = \int_\Omega \mathrm{d}x'\mathrm{d}y' G_{xx}(x-x', y-y')\sigma_{xz}(x', y') + \int_\Omega \mathrm{d}x'\mathrm{d}y' G_{xy}(x-x', y-y')\sigma_{yz}(x', y') \tag{6}$$

$$u_y(x,y) = \int_\Omega \mathrm{d}x'\mathrm{d}y' G_{yx}(x-x', y-y')\sigma_{xz}(x', y') + \int_\Omega \mathrm{d}x'\mathrm{d}y' G_{yy}(x-x', y-y')\sigma_{yz}(x', y'), \tag{7}$$

where

$$G_{\cdot,\cdot}(x,y) = G^0_{\cdot,\cdot}(x,y,z=0), \tag{8}$$

and by abuse of notation,

$$\sigma_{xz}(x,y) = \sigma_{xz}(x,y,z=0) \quad \sigma_{yz}(x,y) = \sigma_{yz}(x,y,z=0). \tag{9}$$

Note that tangential stresses can lead to displacement data in the normal direction.

SETUP OF INVERSE PROBLEM

Here, we develop an objective function for which the minimizing solution provides a good approximation to the underlying stress field, while preserving discontinuities. The first component is simply a quadratic data mismatch term defined by the sum over the displacements measured at the N measurement positions at $\mathbf{r}_i$:

$$\Phi_{\text{data}}[\boldsymbol{\sigma}] = \sum_i^N |\mathbf{u}^{\text{data}}(\mathbf{r}_i) - \mathbf{u}(\mathbf{r}_i)|^2. \tag{10}$$

Since $\mathbf{u}^{\text{data}}(\mathbf{r}_i)$ is given, and $\mathbf{u}(\mathbf{r}_i)$, is given by Eqs. 6 and 7, this contribution to the objective function is a functional over the surface-stress function $\boldsymbol{\sigma}(\mathbf{r}_\perp)$. For simplicity, we will assume that the data points are sampled over an uniform grid with coordinates given $\{(x_j, y_k) : j \in \{1, 2, \ldots, J\}, k \in \{1, 2, \ldots, K\}\}$.

In Eqs 6 and 7, we have restricted the domain of integration to the extent of the cell, Ω, to emphasize that $\boldsymbol{\sigma}$ has compact support. As a consequence of compact support, for a fixed, discretized approximation of σ_{xz}, σ_{yz}, the displacements can be obtained exactly by solving an equivalent system of linear equations of finite dimension.

Here we explicitely define this system of linear equations given a piecewise-affine approximation of the stress field. Let us consider the first-order approximation of σ_{xz} and σ_{yz} using central finite differences, for $x \in [x_j - \delta x/2, x_j + \delta x/2) \cap y \in [y_j - \delta y/2, y_j + \delta y/2)$,

$$\begin{aligned}\sigma_{xz}(x,y) = \sigma_{xz}(x_i, y_j) &+ (x - x_i)\frac{\sigma_{xz}(x_{i+1}, y_j) - \sigma_{xz}(x_{i-1}, y_j)}{2\delta x} \\ &+ (y - y_j)\frac{\sigma_{xz}(x_i, y_{j+1}) - \sigma_{xz}(x_i, y_{j-1})}{2\delta y} \\ &+ \mathcal{O}(\delta x)^2 + \mathcal{O}(\delta y)^2,\end{aligned} \tag{11}$$

where i, j denotes a tuple of grid coordinates. In effect, we are performing sub-pixel interpolation of the stress where the stress is fully-determined by its values at the grid vertices.

Now we may rewrite Eq. 6, for instance, to solve for the displacement at a location (x_n, y_m), by decomposing the integral into a sum of integrals over grid cells

$$
\begin{aligned}
&u_x(x_n, y_m) = \\
&\sum_{(x_j,y_k)\in\Omega} \Bigg\{ \left[\sigma_{xz}(x_j,y_k) - x_j \left(\frac{\sigma_{xz}(x_{j+1},y_k) - \sigma_{xz}(x_{j-1},y_k)}{2\delta x} \right) - y_k \left(\frac{\sigma_{xz}(x_j,y_{k+1}) - \sigma_{xz}(x_j,y_{k-1})}{2\delta y} \right) \right] \langle G_{xx} \rangle^{nmjk} \\
&\quad + \left[\frac{\sigma_{xz}(x_{j+1},y_k) - \sigma_{xz}(x_{j-1},y_k)}{2\delta x} \right] \langle x G_{xx} \rangle^{nmjk} + \left[\frac{\sigma_{xz}(x_j,y_{k+1}) - \sigma_{xz}(x_j,y_{k-1})}{2\delta y} \right] \langle y G_{xx} \rangle^{nmjk} \\
&\quad + \left[\sigma_{yz}(x_j,y_k) - x_j \left(\frac{\sigma_{yz}(x_{j+1},y_k) - \sigma_{yz}(x_{j-1},y_k)}{2\delta x} \right) - y_k \left(\frac{\sigma_{yz}(x_j,y_{k+1}) - \sigma_{yz}(x_j,y_{k-1})}{2\delta y} \right) \right] \langle G_{xy} \rangle^{nmjk} \\
&\quad + \left[\frac{\sigma_{yz}(x_{j+1},y_k) - \sigma_{yz}(x_{j-1},y_k)}{2\delta x} \right] \int_{y_k-\delta y/2}^{y_k+\delta y/2} \langle x G_{xy} \rangle^{nmjk} + \left[\frac{\sigma_{yz}(x_j,y_{k+1}) - \sigma_{yz}(x_j,y_{k-1})}{2\delta y} \right] \langle y G_{xy} \rangle^{nmjk} \Bigg\}, \quad (12)
\end{aligned}
$$

where

$$
\begin{aligned}
&\langle g(x,y) G_{st} \rangle^{nmjk} = \\
&\int_{y_k-\delta y/2}^{y_k+\delta y/2} \int_{x_j-\delta x/2}^{x_j+\delta x/2} g(x',y') G_{st}(x_n - x', y_m - y') \mathrm{d}x' \mathrm{d}y', \quad (13)
\end{aligned}
$$

except that at the edges where we use one-sided differences so that we are only differentiating within Ω. Explicit closed-form expressions for the integrals represented by Eq. **??** are given in the Supplemental Materials. A similar expression can be found for solving for u_y (not shown).

Regrouping terms, we can now define the linear system of equations for solving for u_x at all grid points simultaneously,

$$
u_x^{nm} = X^{nmjk} \sigma_{xz}(x_j, y_k) + Y^{nmjk} \sigma_{yz}(x_j, y_k), \quad (14)
$$

where summation is implied over each index tuple (j,k), and the coefficient matrices are defined as

$$
\begin{aligned}
X^{nmjk} &= \langle G_{xx} \rangle^{nmjk} - \langle G_{xx} \rangle^{n,m,j-1,k} \frac{x_{j-1}}{2\delta x} \\
&\quad + \langle G_{xx} \rangle^{n,m,j+1,k} \frac{x_{j+1}}{2\delta x} - \langle G_{xx} \rangle^{n,m,j,k-1} \frac{y_{k-1}}{2\delta y} \\
&\quad + \langle G_{xx} \rangle^{n,m,j,k+1} \frac{y_{k+1}}{2\delta y} - \frac{\langle x G_{xx} \rangle^{n,m,j-1,k}}{2\delta x} \\
&\quad + \frac{\langle x G_{xx} \rangle^{n,m,j+1,k}}{2\delta x} - \frac{\langle y G_{xx} \rangle^{n,m,j,k-1}}{2\delta y} \\
&\quad + \frac{\langle y G_{xx} \rangle^{n,m,j,k+1}}{2\delta y} \quad (15)
\end{aligned}
$$

$$
\begin{aligned}
Y^{n,m,j,k} &= \langle G_{xy} \rangle^{nmjk} - \langle G_{xy} \rangle^{n,m,j-1,k} \frac{x_{j-1}}{2\delta x} \\
&\quad + \langle G_{xy} \rangle^{n,m,j+1,k} \frac{x_{j+1}}{2\delta x} - \langle G_{xy} \rangle^{n,m,j,k-1} \frac{y_{k-1}}{2\delta y} \\
&\quad + \langle G_{xy} \rangle^{n,m,j,k+1} \frac{y_{k+1}}{2\delta y} - \frac{\langle x G_{xy} \rangle^{n,m,j-1,k}}{2\delta x} \\
&\quad + \frac{\langle x G_{xy} \rangle^{n,m,j+1,k}}{2\delta x} - \frac{\langle y G_{xy} \rangle^{n,m,j,k-1}}{2\delta y} \\
&\quad + \frac{\langle y G_{xy} \rangle^{n,m,j,k+1}}{2\delta y}. \quad (16)
\end{aligned}
$$

From the equation-counting perspective, the system of equations is exactly determined given that one has at least as many measurement points as grid cells in the resolution that one wishes to reconstruct the stress field, provided that one is able to measure displacements in both principle directions. However, in line experiments this is not the case. Furthermore, even if one is able to measure both displacements, the problem may still be highly ill-conditioned since measurements are taken in the presence of noise at a a finite precision. To resolve these issues, we introduce the concept of physically consistent regularization as applied to this problem.

Physical regularization

So far, the construction of the surface stress, even at the finite resolution where measurements are available, is ill-conditioned. We regularize this problem, by forcing the reconstruction to obey some physically-relevant characteristics of the surface stress. First, since we are assuming inertial effects are negligible, we require that the net force is zero, or that

$$
\int_\Omega \sigma_{xz}(x,y) \mathrm{d}x\mathrm{d}y = \int_\Omega \sigma_{yz}(x,y) \mathrm{d}x\mathrm{d}y = 0. \quad (17)
$$

Likewise, we require that there is no net torque, or that

$$
\int_\Omega \sigma_{yz}(x,y) x \mathrm{d}x\mathrm{d}y = \int_\Omega \sigma_{xz}(x,y) y \mathrm{d}x\mathrm{d}y. \quad (18)
$$

Finally, we would like to impose regularity on the reconstructed fields while preserving first rotational invariance and second sharp interfaces. To this end we employ a variant of a penalty used often in image processing applications, where we wish to penalize the L^1 norm of the variation in the fields, or the total variation. To do this in such a manner that is consistent with the philosophy that rotation of the data should not affect the result, we penalize the total variation norm of the invariants of the stress tensor. In the case of two-dimensional tensors, of which the surface stress is an example, the tensor invariants are the trace

$$\mathrm{Tr}(\boldsymbol{\sigma}) = \sigma_{xz} + \sigma_{yz} \tag{19}$$

and the determinant

$$\mathrm{Det}(\boldsymbol{\sigma}) = \sigma_{xz}\sigma_{yz}. \tag{20}$$

Any regularization penalty imposed on the reconstruction problem must be a functional of these invariants in order to maintain rotational invariance, relative to the choice of observation frame, of the reconstructed stress tensor.

For this manuscript, we investigate penalty functionals on the trace of the stress tensor. In particular, we are interested in the L^1 norm of the trace

$$\Phi_{L^1(Tr)} = \int_\Omega |\sigma_{xz}(x,y) + \sigma_{yz}(x,y)| \mathrm{d}x\mathrm{d}y \tag{21}$$

and total variation norm of the trace

$$\Phi_{TV(Tr)} = \int_\Omega |\nabla(\sigma_{xz}(x,y) + \sigma_{yz}(x,y))| \mathrm{d}x\mathrm{d}y. \tag{22}$$

Using either of these expressions as a regularization norm Φ_{reg} suggests the penalized optimization problem

$$\hat{\boldsymbol{\sigma}}\big|\lambda = \arg\min_{\boldsymbol{\sigma}} \left\{\Phi_{\mathrm{data}}[\boldsymbol{\sigma}] + \lambda\Phi_{\mathrm{reg}}[\boldsymbol{\sigma}]\right\}, \tag{23}$$

subject to the constraints mentioned above, where $\lambda > 0$ is a tunable parameter. This problem is in a standard form that is directly solvable using a variety of optimization routines. In our implementation, we use a second-order quadratic cone solver.

Reducing computation by using a cut-off

To reduce the size of the system of equations described in Eqs. 14–16, we note that the Green's function falls off at a rate of r^{-1}. However, when combined with the zero-force constraint, the relationship between the displacements and the support of the stress field falls off at the much quicker rate of r^{-2}, under a set of reasonable assumptions that are consistent with the choice of regularization that we have made.

Lemma 1. *Let $\Omega = supp(\boldsymbol{\sigma}) \subset \mathbb{R}^2$ be compact, and assume that $\boldsymbol{\sigma} \in L^1(\Omega)$. For a fixed $\mathbf{x} \notin \Omega$, denote $D(\mathbf{x}) = \inf\{||\mathbf{x} - \mathbf{y}|| : \mathbf{y} \in \Omega\}$. Then, for $\mathbf{x}$ where $D(\mathbf{x}) \geq R > 0$,*

$$|u_x(\mathbf{x})| \leq \frac{C_x\|\boldsymbol{\sigma}\|_1}{R^2} \tag{24}$$

and

$$|u_y(\mathbf{x})| \leq \frac{C_x\|\boldsymbol{\sigma}\|_1}{R^2} \tag{25}$$

for some constants C_x, C_y.

Lemma 2. *Let $\tilde{\boldsymbol{\sigma}}$ be an affine approximation to $\boldsymbol{\sigma} \in C^s(\Omega)$ for $s \in \mathbb{Z}^+$, and $\tilde{\mathbf{u}}$ be the corresponding displacement field completed from the approximate stress field. Then,*

$$|\tilde{\mathbf{u}} - \mathbf{u}| \leq C(\delta x)^2 \tag{26}$$

The decay of the influence of stress on the system provides justification for setting distance-based cut-offs specification of the linear system. The effect of the cut-off is to limit the left-hand side of Eq. 14 to only locations within some maximal distance R from the outline of the cell. The error in the solution of the inverse problem is dependent on the precision of the observations, the physical constants that describe the medium, and the maximum magnitude of the stress.

Theorem 3. *Denote $\varepsilon^R(\mathbf{x}) = \hat{\boldsymbol{\sigma}}^R(\mathbf{x}) - \boldsymbol{\sigma}(\mathbf{x})$ for $\mathbf{x} \in \Omega$, where $\sigma_{xz} \in L^1(\Omega)$, and $\hat{\boldsymbol{\sigma}}^R(\mathbf{x})$ is the reconstructed stress field found by solving the optimization problem of Eq. 23 using only the displacement data within a maximal distance of R from the cell. Then,*

$$\sup|\hat{\boldsymbol{\sigma}}^R(\mathbf{x}) - \hat{\boldsymbol{\sigma}}^\infty(\mathbf{x})| \leq \frac{C}{R^2} \tag{27}$$

Proof. TODO... result needs refinement

□

COMPUTATIONAL INVESTIGATION

We implemented our regularized inversion method in Python version 3.5, where optimization is performed using the `cvxpy` package with the `ecos` solver. Our implementation can be found at `https://github.com/joshchang/tractionforce`. As a test, we used this method to reconstruct the force field for a dataset where the surface displacements are only known along a single axis, denoted x. TODO DESCRIBE MORE ABOUT THE DATA USED... WHAT IT IS OF AND WHERE IT IS FROM

The results of this test are shown in Fig. 2. Here, we have compared reconstruction of the surface stress using our rotationally invariant norms of Eq. 21 and Eq. 22

FIG. 2. **Reconstruction of surface stress field** for various choices of regularization. The first and third rows are physically-consistent regularizations. The best reconstruction balances regularity and data matching and corresponds to the value for λ that is near a phase transition in the trade off plot between these two penalties (circled in red). The under-regularized solution corresponds to the point circled in green and the over-regulated solution corresponds to the point circled in black.

against alternate isotropic norms. As an alternative to the L^1 norm on the trace we compared

$$\Phi_{L1} = \int_\Omega |\sigma_{xz}(x,y) + \sigma_{yz}(x,y)| \, \mathbf{dx}, \tag{28}$$

and as alternatives to the total variation on the trace we looked at

$$\Phi_{TV_1} = \int_\Omega (|\nabla\sigma_{xz}(x,y)| + |\nabla\sigma_{yz}(x,y)|) \, \mathbf{dx} \tag{29}$$

and

$$\Phi_{TV_2} = \int_\Omega (|\partial_x\sigma_{xz}| + |\partial_y\sigma_{xz}| + |\partial_x\sigma_{yz}| + |\partial_y\sigma_{yz}|) \, \mathbf{dx}. \tag{30}$$

The adjustable parameter λ was chosen in each instance by examining the balance between data mismatch and regularity using trade-off curves shown in Fig. 2, and taking the value for λ that yields a point farthest away from the line segment joining the ends of the plot. In Fig. 2, the chosen value of λ corresponds to the given balance between regularity and data fidelity marked by the red circle. The solution corresponding to this particular value of λ is shown in the middle column on the right. For reference, under-regularized solutions, corresponding to the green circle in the trade-off plot, and over-regularized solutions, corresponding to black circle, are also given. Each row in Fig. 2 corresponds to the use of a different regularization penalty functional. In all of these reconstructions, we have imposed that the surface stress is both force-free and torque free, and also that the support of the stress is within given cell boundaries.

To explore the effect of the constraints on our reconstructions, we systematically removed them in solving the rotationally invariant L^1 regularized problem In Fig. 3, we present reconstructions where net torque is free to vary but force is constrained, where net force is free to vary but torque is constrained, and where net torque and force are both free to vary. In each of these reconstructions the unconstrained quantity did not sum to zero, as desired.

Additionally, our reconstructions are implicitly constrained by the assumption of compact support where the support of the stress tensor is within the cell boundary. Examining Fig. 2, it appears that this constraint is active as much of the stress is concentrated at boundaries. In Fig. 4, we loosened the boundary constraint by allowing the support of the stress to fall within 10 pixels of the cell boundary.

FIG. 3. **Omission of constraints** leads to solutions that do not naturally obey the constraints. Plotted are best reconstructions under the isotropic L^1 penalty and the difference between these reconstructions and the corresponding fully constrained reconstruction of Fig. 2.

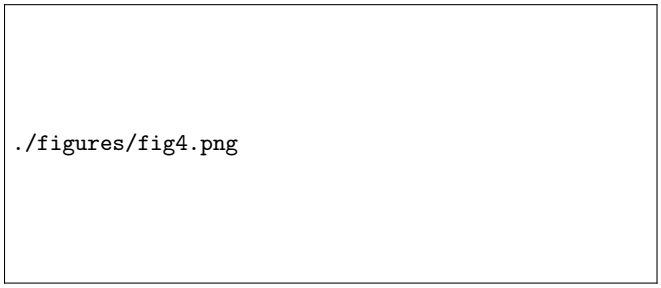

FIG. 4. **Boundary constraint weakening** leads to solutions where the support does not fall naturally within the cell boundary. In the unconstrained reconstruction, the support of the stress was allowed to extend an additional 10 pixels outside of the cell boundary. The reconstruction did not naturally limit its support to the cell boundary.

DISCUSSION

We have presented a comprehensive method for solving the inverse problem of surface stress reconstruction the incorporates physical knowledge as constraints. Under piecewise affine approximations of the stress tensor, we provided an exact solution to the forward problem as a system of linear equations. Using the multipole expansion, we motivated the use of a cut-off in the solution of the forward problem that greatly reduces the rank of the inverse problem thereby decreasing both the computational complexity of the problem and the memory requirements. The numerical stability of the problem was also improved using regularization which obeyed the physical knowledge that the problem should be rotationally invariant.

SUMMARY AND CONCLUSIONS

[1] James HC Wang and Jeen-Shang Lin. Cell traction force and measurement methods. *Biomechanics and modeling in mechanobiology*, 6(6):361–371, 2007.

Integrals

In this section we provide closed-form expressions for the integrals represented by Eq. 13. Let $\Delta x^+_{nj} = x_n - (x_j + \delta x/2)$, $\Delta x^-_{nj} = x_n - (x_j - \delta x/2)$, $\Delta y^+_{mk} = y_m - (y_k + \delta y/2)$, and $\Delta y^+_{mk} = y_m - (y_k - \delta y/2)$. Then, we have the averaged Greens functions

$$\langle G_{uv}\rangle^{nmjk} = f_{uv}(\Delta x^+_{nj}, \Delta y^+_{mk}) - f_{uv}(\Delta x^+_{nj}, \Delta y^-_{mk}) - f_{uv}(\Delta x^-_{nj}, \Delta y^+_{mk}) + f_{uv}(\Delta x^-_{nj}, \Delta y^-_{mk}) \tag{31}$$

where

$$f_{xx}(x,y) = \frac{\nu+1}{\pi E}\left[x(1-\nu)\log\left(\sqrt{x^2+y^2}+y\right) + y\log\left(\sqrt{x^2+y^2}+x\right) - y\right] \tag{32}$$

$$f_{yy}(x,y) = \frac{\nu+1}{\pi E}\left[y(1-\nu)\log\left(\sqrt{x^2+y^2}+x\right) + x\log\left(\sqrt{x^2+y^2}+y\right) - x\right] \tag{33}$$

$$f_{xy}(x,y) = -\frac{\nu(\nu+1)}{\pi E}\sqrt{x^2+y^2}. \tag{34}$$

The first moments follow

$$\langle xG_{xx}(x,y)\rangle^{nmjk} = \Big[f_{xx}(\Delta x^+_{nj}, \Delta y^+_{mk}) - f_{xx}(\Delta x^+_{nj}, \Delta y^-_{mk}) - f_{xx}(\Delta x^-_{nj}, \Delta y^+_{mk}) + f_{xx}(\Delta x^-_{nj}, \Delta y^-_{mk})\Big]x_n - \Big[f^x_{xx}(\Delta x^+_{nj}, \Delta y^+_{mk}) - f^x_{xx}(\Delta x^+_{nj}, \Delta y^-_{mk}) - f^x_{xx}(\Delta x^-_{nj}, \Delta y^+_{mk}) + f^x_{xx}(\Delta x^-_{nj}, \Delta y^-_{mk})\Big], \tag{35}$$

where

$$f^x_{xx}(x,y) = \frac{\nu+1}{2\pi E}\Big[(\nu+1)y\sqrt{x^2+y^2} - (\nu-1)x^2\log\left(\sqrt{x^2+y^2}+y\right)\Big], \tag{36}$$

$$\langle yG_{xx}(x,y)\rangle^{nmjk} = \Big[f_{xx}(\Delta x_{nj}^{+},\Delta y_{mk}^{+}) - f_{xx}(\Delta x_{nj}^{+},\Delta y_{mk}^{-}) - f_{xx}(\Delta x_{nj}^{-},\Delta y_{mk}^{+}) + f_{xx}(\Delta x_{nj}^{-},\Delta y_{mk}^{-})\Big] y_m - \Big[f_{xx}^{y}(\Delta x_{nj}^{+},\Delta y_{mk}^{+}) - f_{xx}^{y}(\Delta x_{nj}^{+},\Delta y_{mk}^{-}) - f_{xx}^{y}(\Delta x_{nj}^{-},\Delta y_{mk}^{+}) + f_{xx}^{y}(\Delta x_{nj}^{-},\Delta y_{mk}^{-})\Big], \tag{37}$$

where

$$f_{xx}^{y}(x,y) = \frac{\nu+1}{2\pi E}\left[y^2\log\left(\sqrt{x^2+y^2}+x\right) - \sqrt{x^2+y^2}\left((2\nu-1)x+\frac{1}{2}\sqrt{x^2+y^2}\right)\right], \tag{38}$$

and

$$\langle xG_{xy}(x,y)\rangle^{nmjk} = \Big[f_{xy}(\Delta x_{j}^{-},\Delta y_{k}^{+}) - f_{xy}(\Delta x_{j}^{-},\Delta y_{k}^{-}) - f_{xy}(\Delta x_{j}^{+},\Delta y_{k}^{+}) + f_{xy}(\Delta x_{j}^{+},\Delta y_{k}^{-})\Big] x_n - \Big[f_{xy}^{x}(\Delta x_{j}^{+},\Delta y_{j}^{+}) - f_{xy}^{x}(\Delta x_{j}^{+},\Delta y_{j}^{-}) - f_{xy}^{x}(\Delta x_{j}^{-},\Delta y_{j}^{+}) + f_{xy}^{x}(\Delta x_{j}^{-},\Delta y_{j}^{-})\Big] \tag{39}$$

where

$$f_{xy}^{x}(x,y) = \frac{\nu(\nu+1)}{\pi E}\Big[\frac{y^2}{2}\log\left(\sqrt{x^2+y^2}+x\right) - \frac{1}{4}\sqrt{x^2+y^2}\left(\sqrt{x^2+y^2}+2x\right)\Big]. \tag{40}$$

All of these expressions may be found through direct iterated evaluation of the integrals, noting that as long as $n \neq m$ or $j \neq k$ the integrand (effectively the Green's function) is bounded, hence making Fubini's theorem applicable given the compactly supported domains of integration.

In the special case where $n = m$ and $j = k$, these formulae also hold. This fact is found by decomposing the integration domain to exclude the origin, for instance in the manner

$$\int_{-\Delta y/2}^{\Delta y/2}\int_{-\Delta x/2}^{\Delta x/2}\mathbf{dx} = \lim_{\varepsilon\to 0}\left(\int_{\varepsilon}^{\Delta y/2} + \int_{-\Delta y/2}^{\varepsilon}\right)\int_{\Delta x/2}^{\Delta x/2}\mathbf{dx}. \tag{41}$$

Since the antiderivatives of Eqs 32, 33, 34, 36, 38, and 40 all have well-defined limits with only removable discontinuities at the origin, integrals of the Green's functions defined through Eq. 41 all converge about the origin and the equations above also hold in the case where $n = m$ and $j = k$.

Proof of Lemma 1

Proof. Note that u_x and u_y are symmetric in form. Hence, it will suffice to prove just one of these assertions. Consider the multipole expansion for u_x at a fixed location $\mathbf{x} \notin \Omega$,

$$u_x(\mathbf{x}) = \sum_{n=0}^{\infty}\frac{U_x(\theta)}{|\mathbf{x}-\mathbf{x}_0|^n}, \tag{42}$$

where $\mathbf{x}_0 \in \Omega$ and $\cos\theta = \frac{(\mathbf{x}-\mathbf{x}_0,\mathbf{x}'-\mathbf{x}_0)}{|\mathbf{x}-\mathbf{x}_0||\mathbf{x}'-\mathbf{x}_0|}$. Eq. 42 is obtained through binomial expansion of the Euclidean distance functions in the denominators of Eq. 3 and Eq. 4,

$$|\mathbf{x}-\mathbf{x}'|^s = |\mathbf{x}-\mathbf{x}_0-(\mathbf{x}'-\mathbf{x}_0)|^s = \left[|\mathbf{x}-\mathbf{x}_0|^2 - 2(\mathbf{x}-\mathbf{x}_0)(\mathbf{x}'-\mathbf{x}_0) + |\mathbf{x}'-\mathbf{x}_0|^2\right]^{s/2}.$$

In particular, since all the Green's functions scale with distance as $|\mathbf{x}-\mathbf{x}'|^{-1}$, we have the following approximation through the binomial expansion

$$\frac{1}{|\mathbf{x}-\mathbf{x}'|} = \frac{1}{|\mathbf{x}-\mathbf{x}_0|}\sum_{n=0}^{\infty}\binom{n-\frac{1}{2}}{n}\left[\frac{2(\mathbf{x}-\mathbf{x}_0)(\mathbf{x}'-\mathbf{x}_0)-|\mathbf{x}'-\mathbf{x}_0|^2}{|\mathbf{x}-\mathbf{x}_0|}\right]^n = \frac{1}{|\mathbf{x}-\mathbf{x}_0|}\left\{1+\frac{2(\mathbf{x}-\mathbf{x}_0)(\mathbf{x}'-\mathbf{x}_0)-|\mathbf{x}'-\mathbf{x}_0|^2}{2|\mathbf{x}-\mathbf{x}_0|} + \mathcal{O}(|\mathbf{x}-\mathbf{x}_0|^{-2})\right\}. \tag{43}$$

Invoking the net force-free constraint, the first few terms of the expansion of Eq. 42 are

$$U_0 = 0 \tag{44}$$

□

Proof of Lemma 2